J. COMBIN. MATH. COMBIN. COMPUT. 127b (2025) 5875--5897

Journal of Combinatorial Mathematics
and Combinatorial Computing
www.combinatorialpress.com/jcmcc

Study on Improving Transmission Line Hazard Monitoring Using AdaBoost Algorithm in Multi-dimensional Data Environment

Hailong Zhao[1], Ruien Zhang[2], Meiyi Huo[3], Peilin Chen[4,✉], Lei Yang[4]

[1] *Chongqing University, Chongqing, 400000, China*

[2] *Jilin Institute of Chemical Technology, Jinlin, Jilin, 132000, China*

[3] *North China University of Water Resources and Electric Power, Zhengzhou, Henan, 450000, China*

[4] *Huazhong University of Science and Technology, Wuhan, Hubei, 430000, China*

ABSTRACT

During the operation of transmission lines, there are sudden failures and a large number of slow-developing, preventable "gradual" failures, which have seriously threatened the safe and stable operation of the transmission system. Based on analyzing the multidimensional environmental factors affecting line safety, the study proposes a method for identifying the operating state of transmission lines based on the AdaBoost integrated learning algorithm, and develops a set of transmission line hidden danger monitoring system. A decision pile based on Ginin indicators is used as a weak classifier, and the hidden danger monitoring results and their confidence levels are output by training and weighted summation of multiple weak classifiers. Using historical data for validation experiments, the proposed method achieves an accuracy of 95.92% in recognizing the operating state of transmission lines, which is a more superior performance compared with traditional machine learning methods. The system can basically realize the hidden danger monitoring of transmission lines, so as to assist the field operation and maintenance personnel of transmission lines to carry out fault investigation, and reduce the transmission line tripping due to the development of hidden danger into fault.

Keywords: AdaBoost algorithm, Ginin index, Decision pile, Hidden danger monitoring, Transmission line

1. Introduction

In recent years, with the high concentration of population, people living and studying for the stability of the power system requirements are increasingly high, therefore, the safety of the power system has

✉ Corresponding author.
E-mail address: chenpeilin@sxdl518.cn (P. Chen).
Received 15 January 2024; Revised 25 March 2024; Accepted 30 November 2024; Published Online 16 April 2025.
DOI: 10.61091/jcmcc127b-323

the corresponding strict requirements. Accompanied by the population, the high concentration of important infrastructure, the grid scale continues to expand, the volume of transmission lines also expanded, the transmission line structure is gradually changing, from the traditional single line structure evolved into a cable overhead mixed frame, the line more than T-connection structure [1-4]. The structure is extremely difficult both for the precise location of the fault point of the line and fault handling. Transmission line faults are partly developed by the line hidden trouble, the main types of hidden trouble for insulator dirt flash, tree shade, bad weather, environmental factors, etc., these hidden troubles lead to fault tripping, insulation defects and other problems, seriously affecting the stability of the transmission line in the operation of the transmission line [5-8]. Early detection of this type of hidden danger can help reduce the probability of line fault tripping.

In the transmission line operation process of the power system, the application of the monitoring system can not only provide the camera storage and transmission of data related functions, but also through the integration of solar power energy design to enhance the stability and sustainability of the system [9-10]. Therefore, the transmission line hazard monitoring system is able to monitor the transmission spot area and the tower base area for a long time and environmental information acquisition, and is able to monitor and identify the need for timely capture monitoring for the intended location [11]. Monitoring system in the main application of the night market primary and secondary dual camera plus PTZ design to enhance the monitoring process for the presentation of the information picture, at the same time, divided into the main and secondary dual camera design structure to meet the daytime for the high-definition acquisition of image information, but also in the night to implement continuous monitoring [12]. Because the PTZ camera has a horizontal 360 °, and vertical up and down 90 ° rotation radius. Therefore, it is able to monitor the transmission line without dead angle, and also able to identify and warn the foreign body hidden danger in the monitoring area in time. In addition to the hardware structure of the transmission line hidden danger monitoring system, in order to better analyze and integrate the data in the monitoring process, it is also necessary to combine the software monitoring system with the core of intelligent computing unit and intelligent recognition algorithm [13-15]. This can provide accurate identification of specific objects in the area for the monitoring system, and play an important role in paving the way for the subsequent addition of manual identification and accurate positioning of hidden dangers. However, in the practical application of the transmission line hidden danger monitoring system, the blind spot and reporting accuracy of the current monitoring system at night are relatively low, and the auxiliary manual inspection mode is still needed to supplement it in extreme environments, which increases the input cost of human and material resources of the monitoring system to a certain extent, and there is a contradiction between the warning and prediction rate of a single threshold and the accuracy of identification, as well as the harm of network attacks in the power grid system [16-19].

With the development of the Internet era, information technology, intelligent technology as the core of the application of intelligent equipment and the construction of the Internet of Things system began to penetrate into more and more areas of industry. In this era of development, technicians should effectively upgrade and transform the transmission line hazard monitoring link in the power network. Not only can the traditional video monitoring and human resources monitoring system in the efficiency and accuracy of the problem to be solved, but also through the construction of intelligent algorithm technology as the core of the new intelligent monitoring system to improve the overall response speed, so that not only can be useful for the multi-dimensional data information for screening and application, but also greatly reduces the overall difficulty of the later inspection system inspection work, and for further promoting the Transmission line intelligent development of the power system to produce far-reaching positive impact [20-22]. Gopakumar et al [23] used monitoring data from phase measurement units on generator buses, combined with spectral analysis for grid fault diagnosis, and used artificial intelligence to classify faults as a means of constituting an intelligent standby monitoring system for transmission line faults. Zheng et al [24] used convolutional neural networks, support vector machines, and Bresenham's algorithm in conjunction with the geometric features of transmission lines to identify construction machinery, line color texture, and foreign objects, respectively, so as to monitor the transmission lines on the alignment. Similarly, Zheng et al [25] achieved image-based monitoring of transmission lines by performing feature extraction based on images of the color, texture, and external shape of the line, segmenting the target image into a uniform grid, and also applying deep migration learning to identify hidden dangers on the outside of the line. Liu et al [26] investigated the effectiveness of the designed transmission tower flood identification algorithm in identifying flood hazards and flood faults in transmission line towers, which takes into account the distance between the flood and the tower, the grid distance of the tower search area, and is able to accurately identify flood hazards within a range of 7 meters. Yang et al [27] supported by artificial intelligence visualization and IOU (Intersection over Union) algorithm, under the deep learning of hidden danger target identification and classification, through the IOU algorithm as a way to overlap the target identification framework to achieve the filtering, and improve the reliability of the transmission line monitoring system. To summarize the study, the accuracy of transmission line hidden danger monitoring and the single-dimensional characteristics of training data need to be improved. The Adaboost (Adaptive Boosting) algorithm builds a strong classifier by iteratively training multiple weak classifiers, each weak classifier focuses on the samples that are classified by the previous classifier, which improves the accuracy of the overall classification, and demonstrates the advantages of self-adaptive selection, interpretability, and small-sample training in the transmission line hidden danger monitoring link [28].

The study utilizes distributed fiber optic sensors to realize the monitoring of hidden dangers of transmission lines, and combines the AdaBoost integrated learning algorithm to design a set of hidden dangers monitoring and warning system for transmission lines. Firstly, the multi-parameter optical time-domain reflectance sensing system (M-OTDR) can simultaneously obtain the Brillouin frequency shift signal and the Rayleigh scattering signal, and realize the simultaneous real-time monitoring of temperature, strain and vibration, so as to grasp the real-time operation status of transmission lines. The overall idea of reducing the transmission line safety hazard warning problem to a classification prediction problem under supervised learning and proposing to take the forecast value of the multidimensional environmental factors triggering the line hazards as the input, and use the AdaBoost integrated learning method as the classifier algorithm to carry out the safety hazard warning of the transmission line. Finally, the actual operation data of circuits are collected to compare the warning effect of this paper's method with that of a single machine learning method to verify the effectiveness of the proposed method.

2. Distributed fiber optic multidimensional data environment for transmission line hazard monitoring

2.1. *Main types of transmission line hazards*

Transmission lines in the long-term operation process by the harsh natural weather, environmental factors, very easy to fault tripping. Through the existing traveling wave method of fault ranging can basically realize stable fault point location and fault detection, however, transmission lines in the long-term operation process, there may be line body or other factors lead to line insulation defects. The main hidden dangers of transmission lines are generally divided into the following types:

First, the long-term growth of trees around the overhead transmission line leads to trees that are super high, which causes the transmission line to discharge due to the influence of wind. Secondly, transmission lines are inevitably affected by natural factors such as lightning strikes during operation, especially lightning currents with small amplitude or lightning currents in the vicinity of transmission lines, which can lead to insulation defects in the insulators of the lines, and although this will not lead to the tripping of the lines in the event of a failure, insulation defects may occur in the event of a long-term full-loaded, high-intensity operation, which may affect the stable operation of the transmission lines. Third, the transmission line in the process of long-term operation of its insulator surface by the accumulation of filth and bird droppings are prone to discharge along the surface of the situation, over the years, resulting in transmission line failure tripped. The insulator surface filth and bird droppings accumulation through manual patrol is generally difficult to identify and investigate. Therefore, it is necessary to identify and warn the hidden danger of overhead transmission lines through scientific and effective means.

2.2. Measurement of multi-parametric optical time-domain reflectance sensing systems

2.2.1. Simultaneous demodulation of Brillouin and Rayleigh backscattered signals. The system structure of M-OTDR is shown in Fig. 1 [29]. The light wave emitted from the narrow linewidth light source is split into two paths by the 90:10 coupler, and 90% of the light is modulated into pulsed light by the intensity modulator, and then amplified by the erbium-doped fiber amplifier (EDFA) and filtered by the optical filter to form a detection pulse of light into the established fiber optic cable for sensing, and the detection pulse of light only needs to occupy a single fiber. Detection of light pulses in the fiber generated by the backscattered signal returned by the circulator into a 50:50 coupler input, the other way 10% of the light as a reference light through the acousto-optic modulator loaded with 40MHz frequency shifted, mixed with the signal light, and through the high-frequency response of the double-balanced detector for outlier coherence detection, and at the same time to get the frequency of 12GHz or so of the RF signal and the 40MHz IF signal mixed signals. The mixed signal of RF signal and 40MHz IF signal is obtained simultaneously.

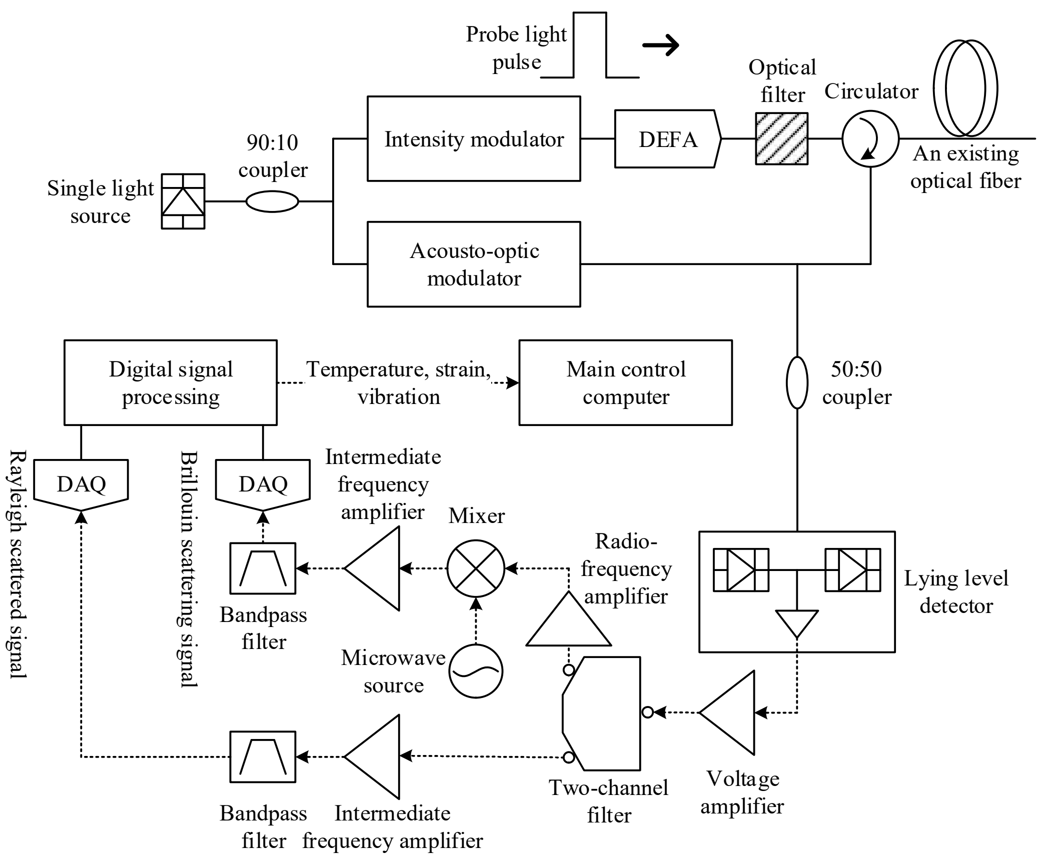

Fig. 1. The system structure of the M-OTDR

2.2.2. Strain measurement based on Brillouin scattering distributed sensing. Compared with Raman scattering signals traditionally used for temperature detection, Brillouin scattering signals are of higher intensity, and since the optical fibers in transmission lines are usually single-mode fibers, BOTDR is particularly suited for high-precision detection of temperature and strain in transmission lines. The amount of change in the Brillouin scattered light frequency shift has the following linear relationship with temperature and strain:

$$\begin{bmatrix} \Delta v_B \\ \dfrac{\Delta P_B}{P_B} \end{bmatrix} = \begin{bmatrix} C_{ot} & C_{oT} \\ C_{Pe} & C_{pT} \end{bmatrix} \begin{bmatrix} \Delta\varepsilon \\ \Delta T \end{bmatrix} \tag{1}$$

Where $\Delta\varepsilon$ and ΔT are the strain change and temperature change, Δv_B is the Brillouin frequency shift change, ΔP_B is the Brillouin power change, P_B is the Brillouin power, C_w and C_{vT} are the strain coefficient and temperature coefficient of the Brillouin frequency shift, and C_{Pe} and C_{PT} are the strain coefficient and temperature coefficient of the Brillouin power, respectively. For ordinary single-mode quartz fiber, when the incident light wavelength is 1550 nm:

$$\begin{cases} C_{ve} = 0.045MHz / \mu e, C_{vT} = 1.2MHz / C \\ C_{P,T} = 0.2985\% / K, C_{P,t} = -11.67\times10^{-4}\% / \mu e \end{cases} \tag{2}$$

The Brillouin scattering signal acquired by the M-OTDR system is the Brillouin scattering spectrum on the distance axis, which can be fitted to obtain the Brillouin frequency shift and Brillouin power on the distance axis, and then the four coefficients of C_{wt}, C_{vT}, C_{pe} and C_{PT} are utilized, thus obtaining the temperature distribution and stress distribution of the transmission line.

2.2.3. Vibration measurement based on Rayleigh scattering distributed sensing. Optical fiber in the steady state, its Rayleigh scattering intensity of the law of change is basically unchanged, can not be eliminated by the traditional cumulative average. However, when a section of the fiber vibration, the corresponding position of the refractive index and length of the fiber will change, and cause the section of the fiber scattering points within the scattered light phase change. The change in the relative phase relationship of the scattered light at each scattering point will result in a fluctuation of the intensity of the backscattered light under interference, and the frequency of the change is highly correlated with the frequency of the external vibration. The position of the vibrating segments can be obtained by measuring the time delay between the injected probe light pulse and the received scattered light signal.

When the coherence of the light source is sufficiently good, the backward Rayleigh scattered light returned by the sensing fiber can be described by a one-dimensional impulse response model, and the electric field strength can be expressed as:

$$E_R(t) = E_s \cos[\omega t + \varphi(t)] \tag{3}$$

Where, E , is the intensity of the signal and ω is the angular frequency of the pulsed light. When a disturbance occurs at a position of the sensing fiber, it induces a change in phase φ, the magnitude of which is positively correlated with the amplitude of vibration, and the modulation to the vibration position after the backward Rayleigh scattered light can be expressed as:

$$E_R(t) = E_s cos[\omega t + \varphi(t) + \varphi_v] \tag{4}$$

From the above equation, it can be seen that the intensity of Rayleigh scattered light changes when the fiber is disturbed by vibration, so the M-OTDR system obtains vibration information by measuring the intensity of scattered light.

2.3. Monitoring of safety hazards

2.3.1. Ice cover monitoring. Distributed fiber optic sensing measures signals that are backward Brillouin scattering signals. At present, the cables laid under the transmission lines are usually of the layer stranded type, and when the relevant parameters of the cables are given, the connection between the fiber optic strain and the fiber optic cable strain can be calculated, so as to convert the monitored fiber optic strain change into the fiber optic cable strain change. Combined with the above calculations to obtain the relationship between the frequency shift and temperature, strain, and in accordance with the performance state of the cable, the cable can be expressed through the formula (5) the size of the stress suffered by the cable:

$$\sigma_w = E\Delta\varepsilon\gamma \tag{5}$$

Where, σ_w is the magnitude of cable stress; E is the Young's modulus of the cable; and $\Delta\varepsilon$ is the magnitude of cable strain change. Since the cable is part of the transmission line in the real transmission line construction process, the initialized installation stress and temperature of the cable on the whole transmission line can be obtained according to the parameter data of its erection.

When the overhead line of the transmission line is in operation, the equation of state of the overhead line in Eq. (6) can be used to obtain the change of its horizontal stress and specific load when the external environment is changed:

$$\sigma_w - \frac{E\gamma^2 l^2 \cos^3\beta}{24\sigma_w^2} = \sigma_{w0} - \frac{E\gamma^2 l^2 \cos^3\beta}{24\sigma_w^2} - \alpha E\cos\beta(T_2 - T_1) \tag{6}$$

Where, σ_{u0}, T_1 for the initial installation stress and temperature of the cable; l for the cable pitch; β indicates the pitch height difference angle; γ for the formula (6) to obtain the specific load of the cable after the uneven ice cover; σ_w for the uneven ice cover after cable

At this point, assuming that the cable diameter is d, the ice density is 0.9 g/cm^3, the thickness of the ice cover is b, at this point, the uneven ice cover after the cable mass per unit length can be expressed by the formula (7):

$$m = \gamma_0 m_0 + 0.9\pi b(b+d)\times 10^{-3} \tag{7}$$

Introducing Eq. (6) into Eq. (7), assuming that the ice cover thickness b is an unknown variable:

$$b = \sqrt{\frac{d^2}{4} + \frac{1000(\gamma - \gamma_0)S}{0.9\pi mg}} - \frac{d}{2} \tag{8}$$

After the solution of Equation (8), the thickness of ice cover can be obtained when the transmission line is single file unevenly covered with ice, so as to realize the transmission line single file unevenly covered with ice monitoring, and maximize the protection of transmission line safety.

2.3.2. Breeze vibration monitoring. At present, the main method to analyze the transmission cable breeze vibration is the energy balance method, the cable under the action of the wind to produce steady-state vibration as a multi-frequency vibration, and that the power induced cable vibration and the power dissipated within the structure is balanced.

Through the above analysis, the cable vibrates both horizontally and vertically caused by the shedding of the Carmen vortex street. Currently, in the study of cable breeze vibration, vibration in the vertical plane is considered to be the dominant vibration, and the horizontal vibration is not taken into account in practice. When modeling cables, the power dissipated within the cable structure is usually considered in practice, mainly by self-damping consumption and the rigidity conditions of the cable itself. In addition, the tensile force on the cable at the exit position for each pitch also affects the vibration pattern of the cable. Considering the actual parameters of the cable, the vibration model in the vertical plane when breeze vibration occurs is usually described by a non-chiral fourth-order partial differential equation:

$$\frac{M_b}{\alpha_c}u^4(x,t)-F_t\frac{\partial^2 u(x,t)}{\partial x^2}+m_L\frac{\partial^2 u(x,t)}{\partial t^2}=q(x,t)+d_\kappa(u(x,t),\frac{\partial u(x,t)}{\partial t},t) \tag{9}$$

Where, M_b for the cable bending moment, α_c for the cable section curvature, bending moment and the ratio of the curvature of the inclined plane can be used as the cable's stiffness, $u(x,t)$ for the cable on the x position at the moment t due to the amount of displacement generated by the breeze vibration, $q(x,t)$ for the cable tail flow in the Kamen vortex in the shedding of the pressure generated by the cable, d_K for the cable itself as well as the damping device located on the cable to jointly produce the damping value.

Equation (9) shows that the stiffness of the cable will directly affect the waveform fitting effect of the breeze vibration. In the actual environment of the wire by gravity fixture stress and other factors will produce arc sag, the actual bending stiffness needs to be estimated empirically. Considering only single-stranded cable arc sag, the calculated cable stiffness value is the lower limit of the theoretical stiffness value:

$$EI_{\min}=\frac{\pi}{64}\sum_{i=1}^{q}E_i d_i^4 \tag{10}$$

Where, $EI_{\min}$: the lower limit of cable stiffness, E_i: the i strand cable modulus of elasticity, d_i: the diameter of the i th cable, q: the number of strands.

If the strands of cable as a whole to consider the cable stiffness, the calculated overall structural stiffness is greater than the actual value, but can be obtained in this way stiffness upper limit:

$$EI_{\max}=\frac{\pi}{4}\sum_{i=1}^{q}E_i(\frac{d_i^4}{16}+d_i^2 a_i^2) \tag{11}$$

Where, $EI_{\max}$: the upper limit of cable stiffness, a_i: the vertical direction of the neutral axis of the cable structure from the center of the cross-section of the i strand cable.

Equation (10) and (11) describe the upper and lower limit values of cable stiffness in the limit case, and the actual bending stiffness of the cable is estimated empirically between $EI_{\min}$ and $EI_{\max}$.

In the previous section has been analyzed Kamen vortex street in the tail flow from the cable will be produced in the cable surface pressure, resulting in oscillation of the cable, in order to facilitate the analysis of the cable is to do the cylindrical dun body, the direction of its force, the size of the cyclic with the vortex in the direction of the change in the direction of the airflow, can be expressed as follows:

$$q(x,t)=\frac{1}{2}C_y d_c \rho_a V_w(x,t) \tag{12}$$

In the formula, C_y for the cable lift coefficient, the first cable structure, state and material effects, $V_w(x,t)$ for the wind speed, the cable at different locations on the wind speed over time are different, d_c for the cable diameter, for the air density, with the temperature, pressure and other factors.

Cable vibration process of self-damping coefficient will also have an impact on the breeze vibration state, analyze the cable vibration process of cable self-damping on the simple harmonic motion displacement effects and energy loss, while through a large number of experiments on the cable self-damping power to give a more direct way of calculating;

$$P_{SD}=\frac{\pi}{2}Dh_{SD}f_s^4 t^{-\frac{1}{2}}m_L^{\frac{1}{2}}u^2(x,t) \tag{13}$$

Where P_{SD} for the cable's self-damping power, h_{SD} for the cable hysteresis damping constant, when the cable material, structure, winding method, etc. to determine the parameter that is constant.

In summary, the cable breeze vibration in the vertical plane vibration waveform should be damped sinusoidal vibration, and the vibration frequency and the inherent frequency of the cable, wake vortex shedding frequency.

2.3.3. OPGW Lightning Strike Optical Polarization State Monitoring. As a composite overhead ground line integrating fiber optic communication and transmission line lightning protection function, OPGW is composed of ground unit and optical unit. In the event of a lightning strike on a transmission line, its pulsed current generates a strong magnetic field, which causes a drastic change in the polarization state of the transmitted light inside the OPGW, and directly reacts to the lightning current as well as the change in the size of the magnetic field by making the Faraday rotation angle. According to the principle of OPGW, through the continuous monitoring of transmission lines in a non-interruptive way before and after the lightning strike changes in the localization of its OPGW light polarization state transmission line lightning strike monitoring model, OPGW light polarization state transmission line lightning strike monitoring model as shown in Figure 2.

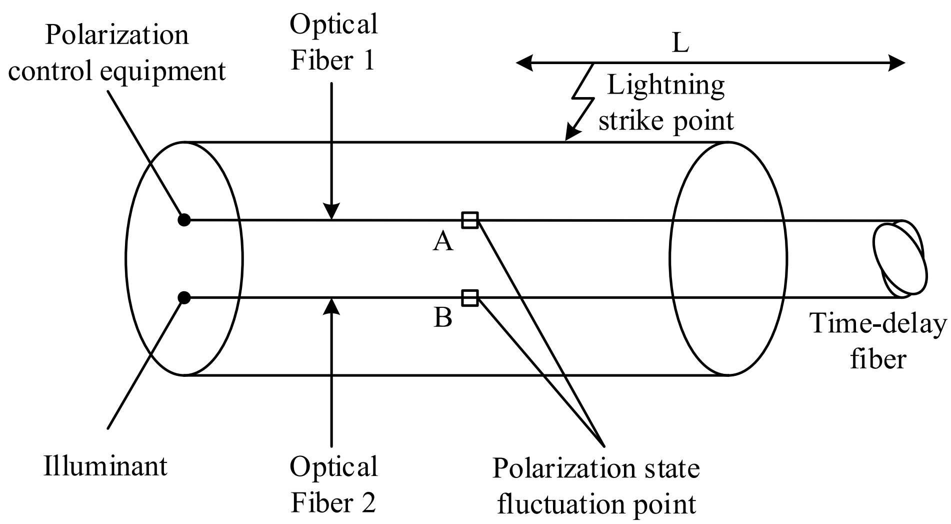

Fig. 2. OPGW optical polarization transmission line road lightning strike monitoring

In the internal OPGW optical polarization state transmission line lightning strike monitoring model corresponding to points A and B, the lightning strike point location exists on two communication fibers, and the light emitted by the laser enters the other fiber in the OPGW through one of the fibers, returns to the beginning, and thus enters the polarization demodulation equipment. After demodulation of the polarization state information by a computer, the time difference between the monitored sudden changes in the polarization state of the transmitted light at points A and B is calculated, so as to measure the distance of the lightning strike point from the midpoint of the tail-end time-delay fiber.

According to the current distribution characteristics on the OPGW optical polarization state transmission line lightning strike monitoring model, its OPGW is connected in parallel with resistance and inductance. Where the spiral component of the current is represented by the inductance, and the through component of the lightning current is represented by the current in the resistance.

When the lightning current in the OPGW is $I(t)$, the wave head and tail times are T_U and T_D, respectively. Its will be $I(t)$ as a power flow, which is calculated as:

$$I(t) = I_0 \left[e^{-\frac{1}{T_D}} - e^{-\frac{1}{T_U}} \right] \tag{14}$$

By calculating the OPGW equivalent circuit, the spiral current component is obtained as:

$$I_L(t) = I_0 \left[\frac{T_U}{\tau - T_U} e^{-\frac{t}{T_U}} - \frac{T_D}{\tau - T_D} e^{-\frac{t}{T_D}} + \frac{(T_D - T_U)\tau}{(\tau - T_D)(\tau - T_U)} e^{-\frac{t}{\tau}} \right] \tag{15}$$

Based on the above calculations, it can be seen that the OPGW current component is mainly affected by the equivalent time constant τ, the wave head time T_υ and the wave tail time T_D. Under the same lightning current waveform, τ in the inductive structure of the OPGW affects the current waveform, while τ along with the OPGW's own parameters affect the results.

3. Transmission line hazard monitoring and early warning system

3.1. AdaBoost integration algorithm

3.1.1. Principles of AdaBoost. For a prediction classification problem, the basic goal of statistical learning is to build learners with strong generalization ability based on observed data. However, in many cases, the fact that the accuracy of the learner is strongly influenced by the domain knowledge and the training data and its distribution (especially for prediction problems whose nature is not yet fully understood, such as wire-over-ice safety hazards) makes it difficult to directly construct learners with high accuracy. However, it is easy to generate several weak learners that are only slightly better than random guesses, so it is valuable to look for general ways to improve the accuracy of existing learners, which provides an effective new way of thinking and approaching the design of learning algorithms when it is very difficult to directly construct strong learners, and it is in this context that integrated learning has emerged.

Since the concept of integrated learning has been proposed, it has been rapidly developed and widely used in many fields. At present, the commonly used integrated learning algorithms are Bagging algorithm (bootstrap aggregation) and Boosting algorithm (augmentation method), and one of the most popular Boosting algorithms is Adaboost (adaptive boosting) algorithm.

The Adaboost algorithm was proposed in 1996 based on the performance analysis of Schapire's "weak classifiers" and Freund's early research on "learning theory" [30]. Since the algorithm does not require prior knowledge of the lower bound of the prediction accuracy of the weak learning algorithm, but only requires that the correct recognition rate of the basic classifier is slightly greater than that of the "random guess" (also known as the weak classifier), it can be better applied to practical problems. It has the advantages of low generalization error rate, easy coding, etc., and is rated as one of the top ten algorithms for data mining.

The basic idea of Adaboost algorithm is to utilize a large number of weak classifiers with general classification ability to be superimposed by certain methods to form a strong classifier with strong classification ability.

The Adaboost algorithm is described as follows:

Inputs: weak classifier design method C; number of training sessions (number of weak classifiers) T; sample set $X=\{(x_1,y_1),(x_2,y_2),\cdots,(x_N,\ldots,(x_N)\rangle y_N)\}$. where x_i is the weather feature vector of the i th sample; $y_i=(-1,1)$ denotes the category labeling of the i th sample: -1 means no safety hazard occurred, 1 means safety hazard occurred, and N is the number of samples.

Initialization: sample weight distribution $w_1(i)=1/N, i=1,2,\cdots,N$.

When $t=1,2,\ldots,T$:

1) Generate a new set of samples X_t from X based on $w_i(i)$ with put-back sampling.
2) Train a weak classifier $C_t(X)$ on X_t and use $C_t(X)$ to classify the original training sample set X.
3) Compute the classification error rate of $C_t(X)$.
4) Calculate the coefficient of $C_t(X)$. I.e:

$$\varepsilon_t=\sum_{i=1}^{N} w_t(i) I(C_t(x_i)\neq y_i) \tag{16}$$

Where: $I(\cdot)$ is 1 when $C_t(x_i)\neq y_i$ and 0 for the rest. ie:

$$a_t = \frac{1}{2}\ln(\frac{1-\varepsilon_t}{\varepsilon_t}) \tag{17}$$

5) Update the weight distribution:

$$w_{t+1}(i) = \frac{w_t(i)}{Z_t} \times \begin{cases} e^{-a_t}, C_t(x_i) = y_i \\ e^{-a_t}, C_t(x_i) \neq y_i \end{cases} = \frac{w_t(i)}{Z_t} \cdot e^{-a_t y_t C_t(x_i)}, i = 1, 2, \cdots, N \tag{18}$$

Where: $Z_t = \sum_{i=1}^{N} w_i(i) \cdot e^{-a} \gamma_i^{C_i(x_i)}$ is the normalization factor which can make $\sum_{i=1}^{N} w_{i+1}(i) = 1$.

6) Final classifier:

$$y = C(X) = \mathrm{sgn}\left[\sum_{t=1}^{T} a_t C_t(X)\right] \tag{19}$$

3.1.2. Construction of weak classifiers. As a weak classifier, simple classifiers are more effective, therefore, the author chooses the most commonly used single layer decision tree as a weak classifier. The decision tree is only based on a single input feature and adopts the threshold division method to make decisions, i.e., there is only one node, and it is also called a decision pile because the tree has only one splitting process, which is similar to the shape of a tree stump.

The most critical problem of decision pile construction is how to judge the threshold division results so as to select the best split point. Currently, the measurement criterion based on the amount of information or the error rate (e.g., Gini metric) is generally used, while the literature points out that the Gini impurity metric performs better than the information metric and is easy to compute, and its most important feature is that only the distribution of the class values in each part of the class at the time of being segmented is taken into account in the computation. Therefore, the author adopts the Gini metric to evaluate the degree of superiority of the segmentation rule, which is defined as follows for dataset S containing c class:

$$gini(S) = 1 - \sum_{j=1}^{c} p_j^2 \tag{20}$$

Where: p_j denotes the proportion of samples of category j in set S. If the partition rule RULE divides S into S_1 and S_2 subsets, the evaluation value of the rule is noted as:

$$gini(S, rule) = \frac{n_1}{n} \cdot gini(S_1) + \frac{n_2}{n} \cdot gini(S_2) \tag{21}$$

Where: n_1 is the number of samples in subset S_1, n_2 is the number of samples in subset S_2, n is the number of samples in set S, and n is the number of samples in set S.

For a numerical attribute, the idea of decision pile segmentation based on Gini index is that after traversing all possible segmentation methods, the one that minimizes the evaluation value $gini(S, rule)$ is chosen as the optimal segmentation rule at this node. The process is described as:

Step1: Sample values of numerical attributes are sorted, assuming that the result after sorting is $(x_1, y_1), (x_2, y_2), \ldots, (x_n, y_n)$.

Step2: Since the segmentation occurs only between 2 data points, the midpoint $(x_i + x_{i+1})/2$ is usually taken as the segmentation point, and then different segmentation points are taken in order from smallest to largest, and the gini value of each segmentation rule is calculated.

Step3: Take the point which minimizes the gini value as the best segmentation point.

3.2. AdaBoost algorithm based transmission line hidden danger warning

The flow of transmission line safety hazard warning based on Adaboost method proposed by the author is shown in Fig. 3.

Finally, based on the margin value of the safety hazard prediction result, the warning level of transmission line safety hazard is set as shown in Table 1.

For the transmission line safety hazard prediction result y obtained from the monitoring input vector x, the confidence level can be calculated by equation (22):

$$margin(x, y) = \frac{\sum_t a_t C_t(x)}{\sum_t |a_t|} \tag{22}$$

Where: $margin \in [-1, +1]$, larger positive (negative) boundaries indicate high confidence in predicting the occurrence (non-occurrence) of safety hazards on the line, while smaller boundaries indicate lower confidence in the prediction results.

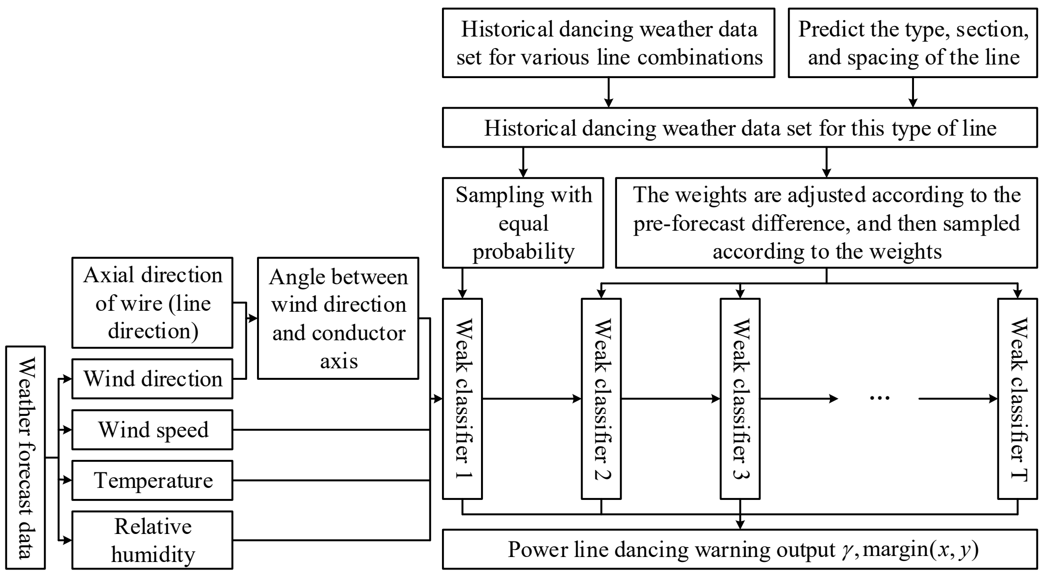

Fig. 3. Flow chart of early warning for transmission line

Table 1. Safety hazard warning grade

Condition	Grade
margin > 0.7	**Grade I**
0.4 < margin ≤ 0.7	**Grade II**
0.1 < maxgin ≤ 0.4	**Grade III**

3.3. Online monitoring system for hidden dangers

3.3.1. Main architecture. The main component of the overhead transmission line hazard monitoring system is the on-site monitoring terminal. The field monitoring terminal is installed on the overhead conductor of the transmission line and is responsible for collecting the discharge data in the overhead transmission line. The monitoring device collects the data and then transmits the data to the remote server through wireless communication. The remote server carries out system analysis and theoretical calculation on the data collected by the terminal, and provides active warning when there are many hidden discharge points in the system, and at the same time pushes the fault data to the designated cell phone terminal and the WEB client used for data display.

3.3.2. Monitoring terminals. The transmission line hidden danger monitoring terminal is installed on the transmission line conductor and is responsible for collecting the discharge signal in the transmission line. The hidden danger discharge generally presents a wide bandwidth, and at the same time, it is necessary to exclude the interference in the strong electromagnetic environment of the transmission line, so the acquisition of the sensor as well as the shielding and subsequent circuitry need to do special treatment. The monitoring device adopts the transmission line high potential coupling power supply plus coupling power supply of traveling wave to ensure stable power supply of the system. Due to the perennial exposure to harsh natural environments, the monitoring terminal is manufactured with materials of high protection level.

3.3.3. Hazard monitoring process. Transmission lines are affected by tree height, bird damage, insulator filth, etc., and the lines are very prone to hidden discharges, and when there is a hidden discharge point in the system, scientifically and effectively determining and dealing with the hidden discharge point will help to reduce the fault tripping rate of overhead transmission lines. The warning algorithm and process of transmission line hidden danger monitoring system are shown in Figure 4.

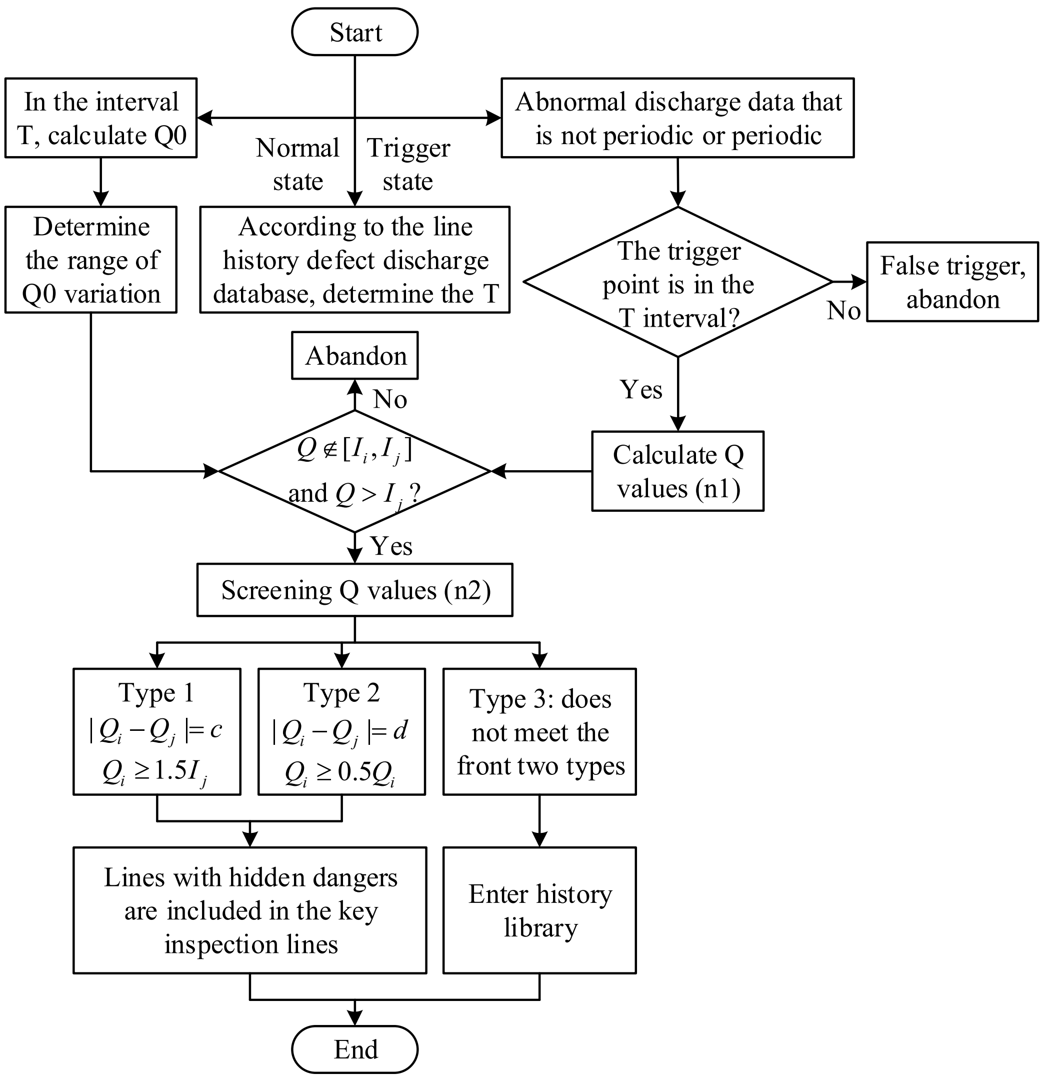

Fig. 4. The warning algorithm and process of the monitoring system of transmission line

The length of the IF waveform collected by the monitoring terminal is selected, t_i is the starting moment of IF, t_j is the ending moment of IF; Q_0 is the base value of hidden trouble discharge in cc; I_i is the minimum current value of hidden trouble discharge, I_j is the maximum current value of hidden trouble discharge; n_1 is the number of discharges in the interval, and n_2 is the number of discharges larger than the maximum amplitude of discharge current I_j. If the discharge current and the number of discharges meet, it can be determined that there is a hidden problem discharge in the line.

1) In 1 to n of the Q values of any two numbers, recorded as Q_i and Q_j, if the Q value and I_j value of the difference is large and meet the relationship between the formula (23), you can determine the existence of hidden discharge line:

$$|Q_i - Q_j| = c \tag{23}$$

$$Q \geq 1.5 I_j \tag{24}$$

where the range of c values is: $0 \leq c \leq 0.1\max(Q_i, Q_j)$.

2) In 1 to l and m to n Q values, each take the value of two numbers, recorded as Q_i and $Q_j, 1 \leq l < m \leq n$, if there are a number of consecutive Q_i and Q_j to satisfy the relationship of formula (25), you can determine that the line is hidden:

$$Q_i - Q_j = d \tag{25}$$

Where the range of d value is: $d \geq 0.5 Q_i$.

Overhead line to meet the above two different discharge conditions are determined as the line there is a hidden problem discharge, according to the principle of double-ended traveling wave localization can be accurately locate the fault point.

4. Monitoring and early warning analysis of transmission line safety hazards

4.1. Analysis of actual operational data

At present, the multi-parameter distributed fiber optic host has been installed in a power supply bureau in the northern part of GD province, the multi-parameter distributed fiber optic device host is directly installed in the substation, access to the optical fiber within the OPGW can be directly carried out multi-operating condition monitoring and fault location, debugging and maintenance is very convenient, the distributed fiber optic host has its own operating system, which is convenient for storing data and remote operation, compared with other online monitoring equipment can save a lot of maintenance and debugging costs. Compared with other online monitoring equipment, it can save a lot of maintenance and commissioning costs.

4.1.1. Analysis of measured line data during periods of ice cover. The wind speed monitoring along the transmission line is calculated by the formula in section 2.3, which collects the wind speed in one minute, in which the average wind speed and maximum wind speed obtained from the equipment monitoring are compared with the wind speed obtained from the micrometeorology as shown in Figure 5. In one minute, the wind speed obtained from equipment monitoring ranges from 0 to 14 m/s, which can accurately get the real-time wind speed details of the line.

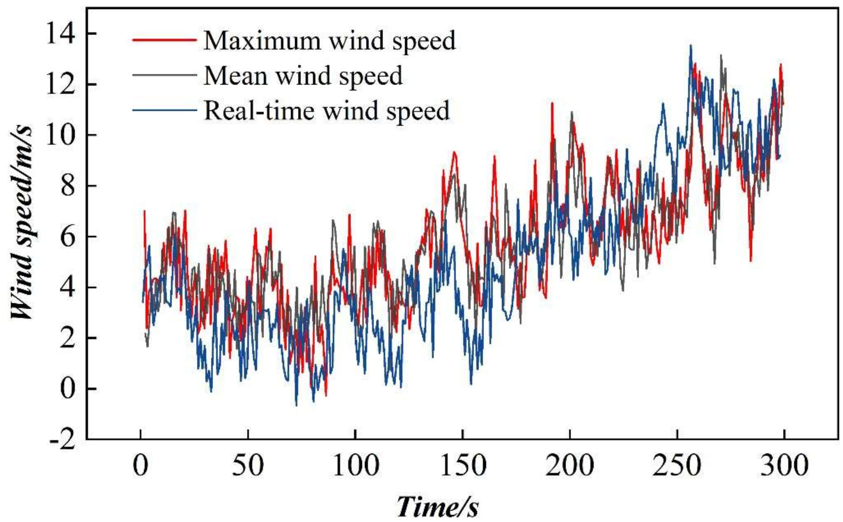

Fig. 5. Wind velocity contrast

Setting 300 gear distance, Figure 6 for the line at 21:30 on March 22, 2023, the moment of each gear distance ice thickness, temperature and wind speed with time change curve. From the figure can be observed that the 150-170 tower ice cover is the most serious, at this time the temperature in -3 ℃ ~ 2 ℃, wind speed in 4 ~ 10m / s, belongs to the key affected areas need to strengthen monitoring.

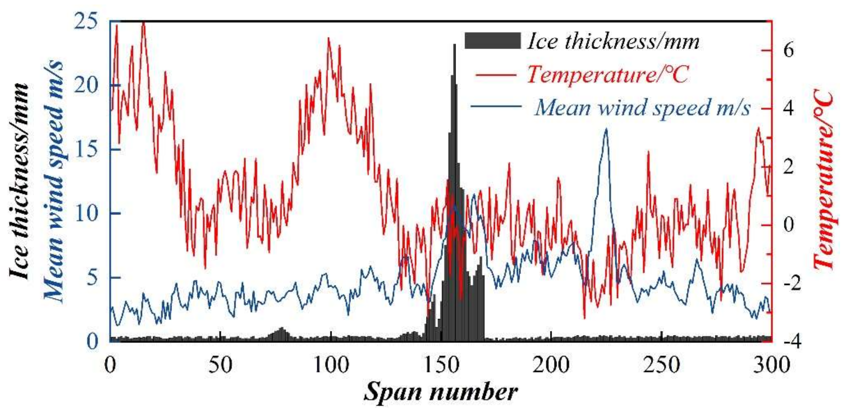

Fig. 6. The distribution curve of ice thickness, temperature and wind speed

The most seriously affected #153 is specifically analyzed, and Fig. 7 shows the graphs of ice cover thickness, wind speed and temperature in the area of the most seriously affected pole tower #153, and (a) and (b) are the monitoring data on the 22nd and 23rd, respectively. It can be obtained that the temperature of pole tower #153 fluctuates around 0℃, and the ice cover thickness is calculated based on the formula of intrinsic frequency-ice cover thickness. In addition, the on-site inspectors also compared the transmission line heavy condition monitoring data with manual weighing, and according to the feedback from the on-site personnel, the ice-covering data of the transmission line heavy condition on-line monitoring device is more consistent with the actual ice-covering situation on the site. Transmission line large conditions online monitoring device can accurately reflect the actual line ice cover, effectively guide the operation and maintenance personnel of the anti-ice work arrangements.

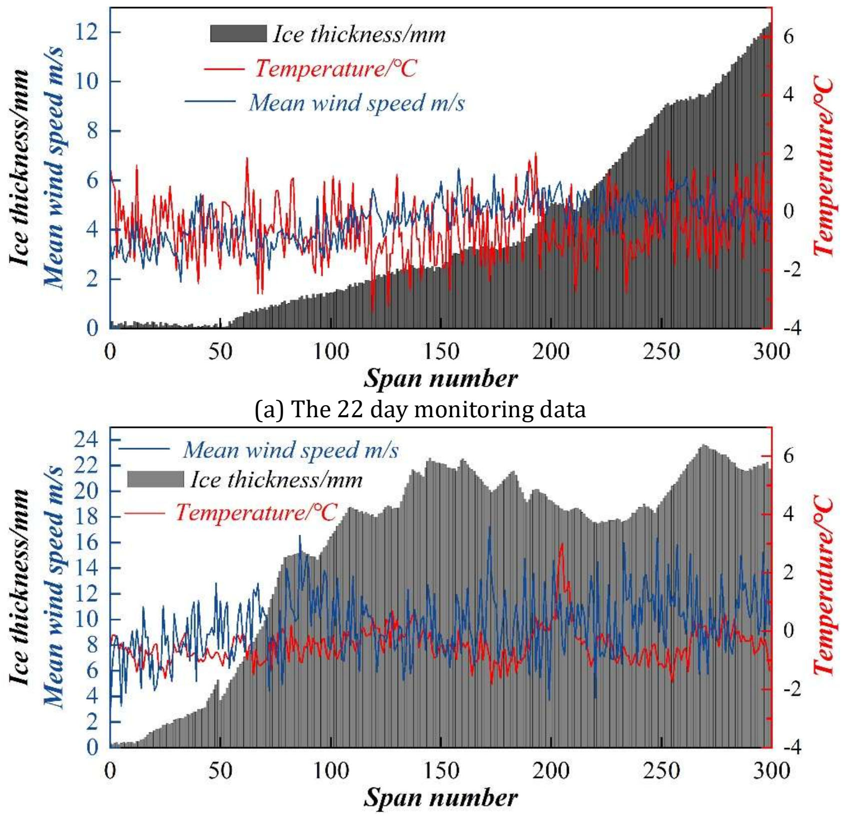

(a) The 22 day monitoring data

(b) The 23 day monitoring data

Fig. 7. The curve of ice thickness, temperature and wind speed with time

4.1.2. Analysis of measured lightning strike data. Figure 8~Figure 10 for a local distributed fiber optic equipment in 220kV line moment point measured during the lightning strike host and slave optical polarization state data, as shown by the figure appears more than one lightning strike counterattack peaks, select the last peak curve for amplification, and then the curve for denoising, smoothing and take the derivative of the extreme point, the lightning strike signal arrives at the host time of 458.9527ms, lightning strike signal Arrived at the slave time is 459.1125ms, the overall length of the line is 44.95km, using the formula to calculate the cable lightning distance from the host distance of 6012.3m, the distance from the slave distance of 39115.2m, the judgment of the lightning location in the tower # 124 ~ # 125 between the location of the actual monitoring of the position and the judgment of the location is the same, the two sets of data to prove that the device is effective in actual line The two sets of data prove that this equipment is effective in the actual line monitoring and positioning of lightning strikes.

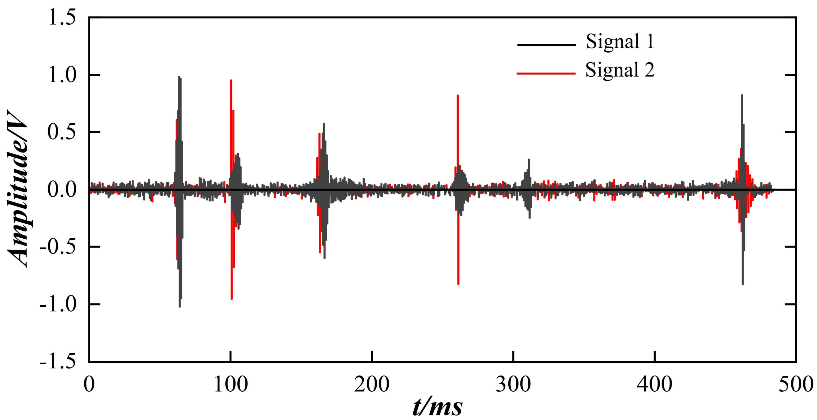

Fig. 8. Lightning shot measured data

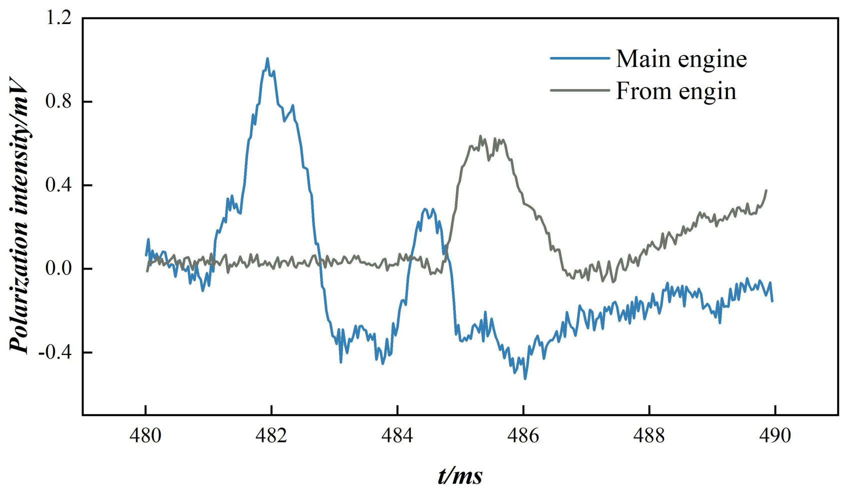

Fig. 9. Local amplification of measured data

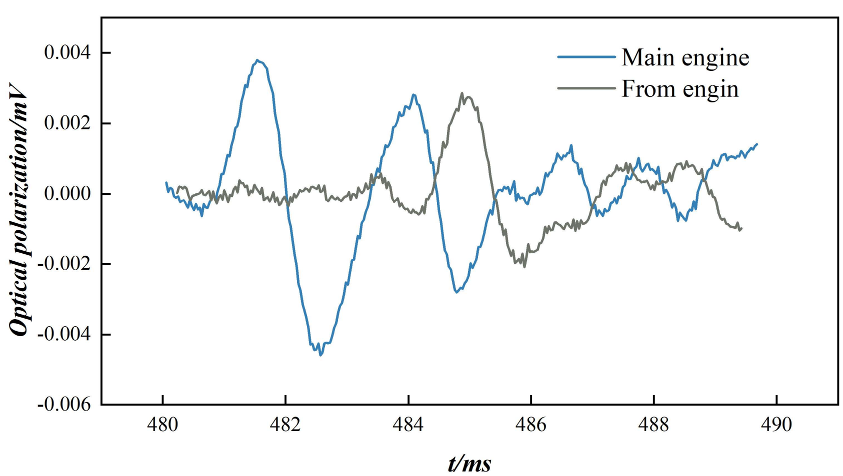

Fig. 10. The curve is smooth and the derivative of the derivative

4.2. Early warning results and discussion

4.2.1. Data sets. Collect 8000 groups of actual running data to form a dataset, and for the 8000 groups of samples in the dataset, divide the training set, testing set and validation set according to the ratio of 7:2:1, i.e., 5600 groups of samples in the training set, 1600 groups of samples in the testing set, and 800 groups of samples in the validation set. The optimizer uses Adam, the initial learning rate is set to 0.01, and in order to make the model quickly converge to the optimal solution, a learning rate decay strategy is added. The loss function is the cross-entropy loss function, the output layer uses the Softmax activation function, the batch size during training is 60, and the maximum number of training times Epoch is 40.

4.2.2. Effect of CWT parameters on recognition results. The core idea of CWT is to utilize a wavelet function to perform wavelet decomposition of a signal at different scales and locations. In the conversion process, the wavelet function is an important parameter to determine the CWT results, which determines the shape of the wavelet basis function, and for different types of data, the appropriate wavelet function should be selected to analyze them. In order to select the wavelet function parameters suitable for this paper's dataset, in this section of the experiment using mexh, gaus4, fbsp, cmor and morl a total of five commonly used wavelet function to convert the data, and analyze its impact on the final recognition results.

Using the method proposed in this paper on different datasets for training, in which the input data of the time series branch are uniformly fixed to the original vibration signal data, the input data of the image branch for the use of five different wavelet function methods converted to time-frequency data. The number of model training is set to 40. Fig. 11 shows the training curve of the model on the validation set, (a) and (b) are the accuracy and loss rate curves, respectively. The accuracy and loss value results of the model on the test set are shown in Table 2. The comparison shows that for the time-frequency image dataset made based on the morl wavelet function method, the model has the highest recognition accuracy of 95.39%. Therefore, in this paper, when constructing the time-frequency image dataset, the morl wavelet function is used for CWT conversion to realize more accurate prediction of transmission line safety hazards.

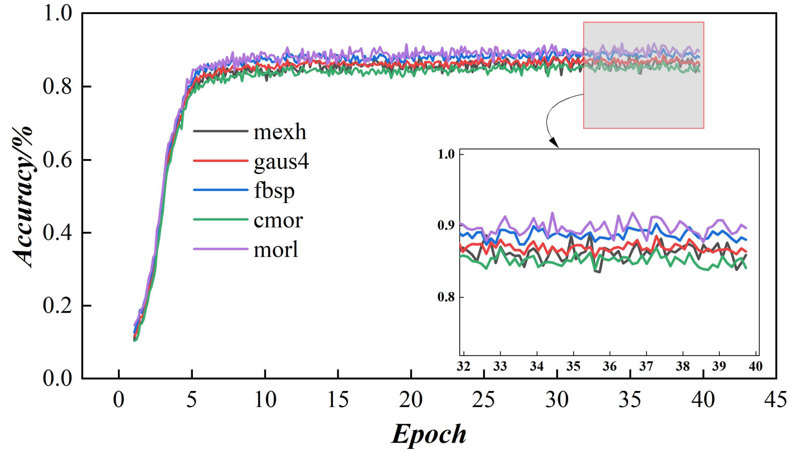

(a)Accuracy rate

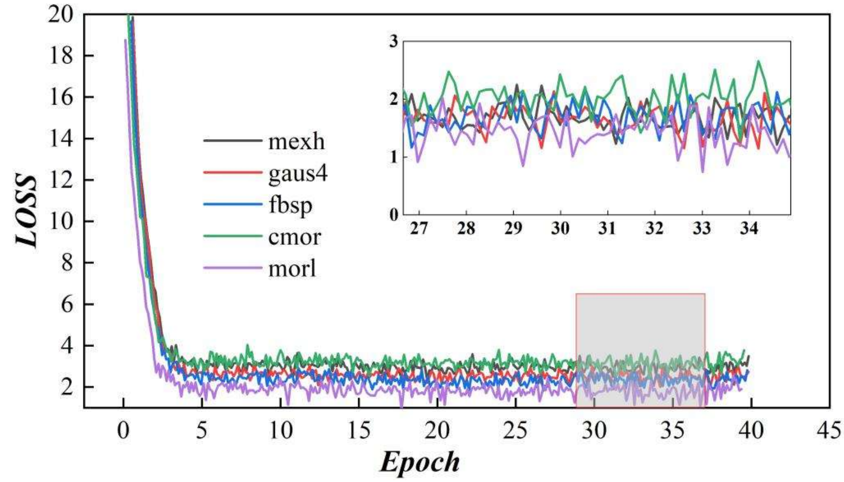

(b) Loss rate

Fig. 11. Model training curve

Table 2. Model recognition results

Wavelet function	Accuracy/%	Loss
mexh	93.44	0.201
gaus4	94.41	0.175
fbsp	92.55	0.222
cmor	93.38	0.213
morl	95.39	0.115

4.2.3. Model comparison experiments. In order to fully verify the superiority of the performance of the model proposed in this paper, it is compared with five single machine learning algorithms, namely, SVM, KNN, decision tree, logistic regression, and plain Bayes, respectively, and the implementations of the machine learning algorithms are all based on Python 3.7 and the third-party module sklearn.For the SVM algorithm, the kernel function is chosen to be RBF, and the optimal penalization factor is determined to be 27 by using the grid search method. For the SVM algorithm, RBF was chosen for the kernel function and the optimal penalty factor was determined to be 27 using the grid search method. Fig. 12 shows the training curves of different models, (a) and (b) are the accuracy and loss rate curves respectively Fig. 13 and Table 3 show the confusion matrix plots of the six models on the test set and the results of evaluation indexes, respectively, (a) to (f) are SVM, KNN, decision tree, logistic regression, plain Bayes and the method of this paper, where in the confusion matrix, 1 to 6 represent ice-covered, wind vibration, lightning strike, tree overheight, heavy rainfall and surface fouling are the six safety hazards.

For the machine model, when constructing the feature dataset, it is not that the more the number of features, the better the recognition results, when the number of features is too much, it may contain certain interference features, but will reduce the recognition performance of the classifier. As far as different classifiers are concerned, the recognition accuracy of plain Bayes is higher than that of KNN and decision tree, and the F1-score value reaches 92.66%, but there is still a big gap compared with the method proposed in this paper, which indicates that there are certain deficiencies in the generalization performance and classification effect of a single machine learning algorithm when dealing with large-scale datasets.

The method proposed in this paper integrates two different modal information, makes up for the respective limitations of one-dimensional vibration signals and two-dimensional image data, and is able to more comprehensively characterize the data features of the safety hazards of transmission lines in a multidimensional environment, and achieves a classification accuracy of 95.92% on the test set, with the best overall evaluation index.

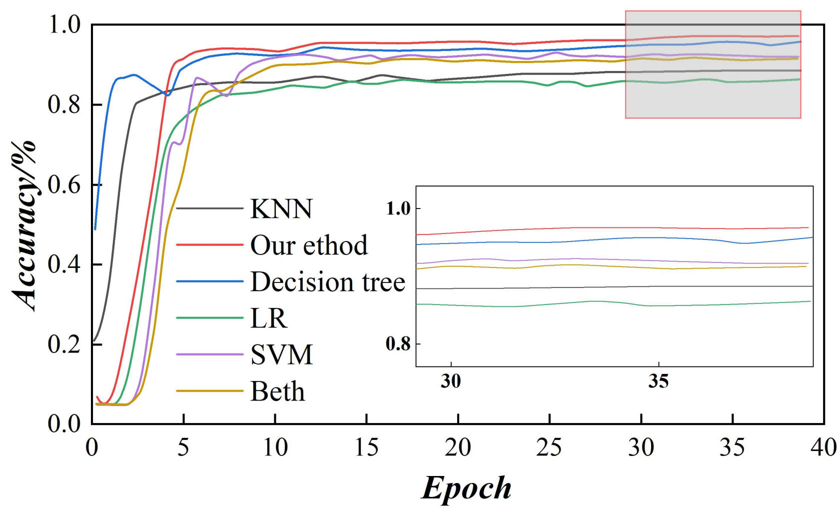

(a) Accuracy rate

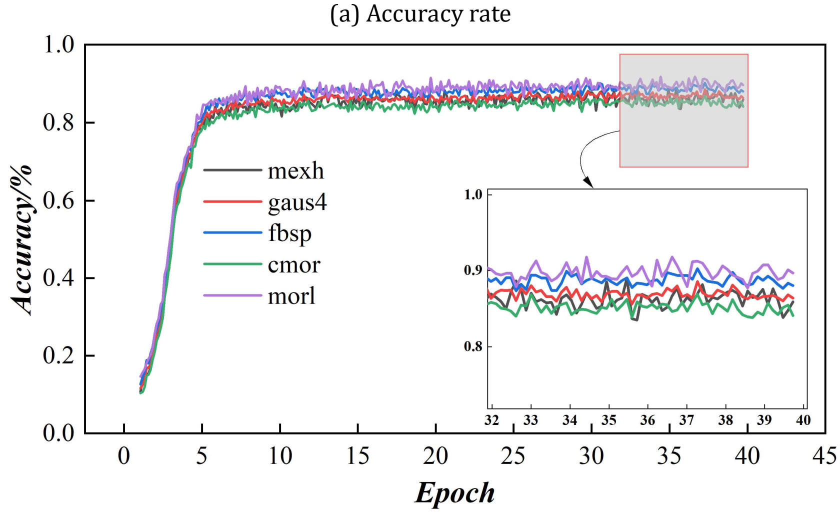

(b) Loss rate

Fig. 12. Six models training curve

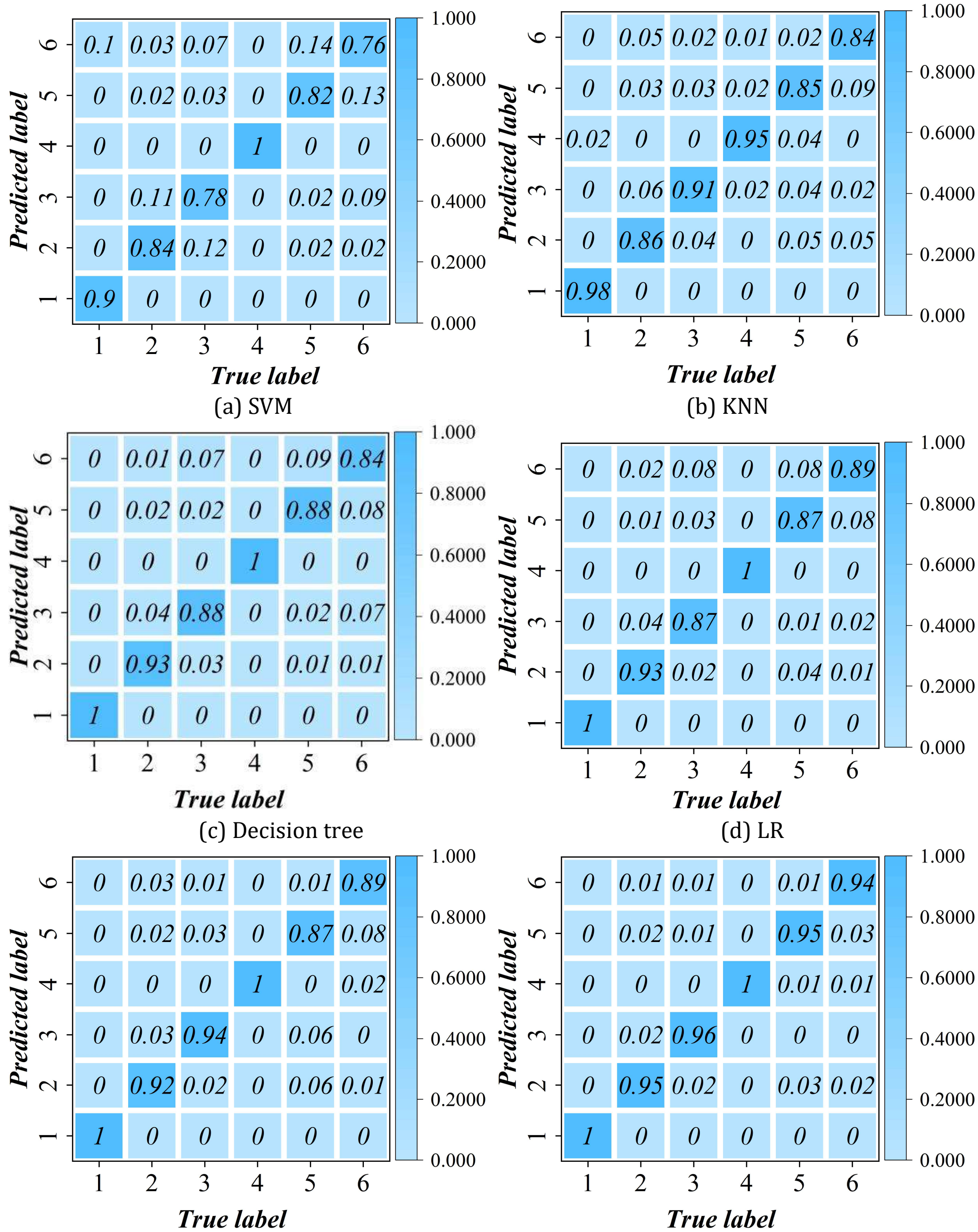

(a) SVM (b) KNN (c) Decision tree (d) LR (e) Beth (f) Our

Fig. 13. Confusion matrix of different models

Table 3. Identification of different models

Model	Accuracy	Precision	Recall	F1-score
SVM	85.75	89.45	85.81	86.92
KNN	90.50	92.72	88.71	90.69
Decision tree	91.13	90.94	87.75	91.31
Beth	92.37	92.93	89.81	92.66
Our	93.64	95.92	93.38	95.49

5. Conclusion

In this paper, according to the requirements of transmission line safety monitoring, AdaBoost algorithm is used to design a set of transmission line multi-condition monitoring system based on multi-parameter distributed fiber optic sensing system, and the physical quantities that can be monitored are temperature, strain, vibration, and electromagnetic field changes of the line and other environments.

Line simulation experiments were carried out using the system and measured line data were collected, and the results show that the system can assess the ice-covering condition of the line by monitoring the strain, temperature and intrinsic frequency of the cable, monitor the wind speed, safety hazards and breeze vibration of the line by vibration, and carry out the strike positioning of the line by using the change of the optical polarization state triggered by the lightning current to realize real-time early warning of the transmission line.

In addition, on the collected dataset, it was compared with five machine learning algorithms, such as SVM, KNN, and decision tree, and the classification accuracy of the proposed method on the test set reached 95.92% and the F1 value was 95.49, which verified that the ensemble model has better generalization and recognition effect on large-scale dataset. The proposed method will provide a useful reference for the operational status monitoring of transmission lines.

Funding

China Southern Power Grid Co., Ltd. Science and technology project (No.: 073000KK52200016).

Author's unit: Hainan Power Grid Co., Ltd., Electric Power Research Institute, Hainan, China, 570311 (Hailong Zhao, Ruien Zhang, Meiyi Huo);

Wuhan Sunshine Power Technology Co., Ltd., Wuhan, Hubei, China (Peilin Chen, Lei Yang).

References

[1] Fairbanks, A. J., Darr, A. M., & Garner, A. L. (2020). A review of nonlinear transmission line system design. IEEE Access, 8, 148606-148621.

[2] El Damatty, A., & Elawady, A. (2018). Critical load cases for lattice transmission line structures subjected to downbursts: Economic implications for design of transmission lines. Engineering structures, 159, 213-226.

[3] Alvarez, R., Rahmann, C., Cifuentes, N., & Palma-Behnke, R. (2021). Multi-year stochastic transmission network expansion planning considering line uprating. IEEE Access, 9, 33075-33090.

[4] Dhamala, B., & Ghassemi, M. (2024). Smart transmission expansion planning based on the system requirements: A comparative study with unconventional lines. Energies, 17(8), 1912.

[5] Cheng, J., Yu, X., & Wu, Y. (2024). Transmission Line Hazard Analysis and Structural Resilience Methods: A Comprehensive Review. Electronics, Communications and Networks, 16-22.

[6] Miguel, L. F. F., Alminhana, F., Brito, J. W. S., Sousa, D. M., & Beck, A. T. (2023). Multi-hazard assessment of transmission line systems subjected to independent non-concurrent turbulent winds and ground accelerations. Structural Safety, 105, 102376.

[7] Liu, Y., Li, B., Wu, C., Chen, B., & Zhou, T. (2021). Risk warning technology for the whole process of overhead transmission line trip caused by wildfire. Natural hazards, 107(1), 195-212.

[8] Davalos, D., Chowdhury, J., & Hangan, H. (2023). Joint wind and ice hazard for transmission lines in mountainous terrain. Journal of Wind Engineering and Industrial Aerodynamics, 232, 105276.

[9] Khawaja, A. H., Huang, Q., & Khan, Z. H. (2017). Monitoring of overhead transmission lines: a review from the perspective of contactless technologies. Sensing and imaging, 18, 1-18.

[10] Cai, C., Wang, J., Liu, R., Fang, Z., Zhang, P., Long, M., ... & Lin, Z. (2018). Resonant wireless charging system

design for 110-kV high-voltage transmission line monitoring equipment. IEEE Transactions on Industrial Electronics, 66(5), 4118-4129.

[11] Suresh, S., Nagarajan, R., Sakthivel, L., Logesh, V., Mohandass, C., & Tamilselvan, G. (2017). Transmission line fault monitoring and identification system by using Internet of Things. International Journal of Advanced Engineering Research and Science (IJAERS), 4(4), 9-14.

[12] Xu, H., Wang, C., Huang, H., & Zeng, Z. (2022, August). Application of 3D Scene Fusion in Transmission Line Video Monitoring. In 2022 International Conference on Artificial Intelligence in Everything (AIE) (pp. 168-173). IEEE.

[13] Sun, R., & Wang, C. (2025). Research on Machine Learning Assisted Hidden Danger Identification and Defect Analysis in Transmission Line Monitoring. In Intelligent Manufacturing and Cloud Computing (pp. 492-497). IOS Press.

[14] Ferreira Dias, C., de Oliveira, J. R., de Mendonça, L. D., de Almeida, L. M., de Lima, E. R., & Wanner, L. (2021). An iot-based system for monitoring the health of guyed towers in overhead power lines. Sensors, 21(18), 6173.

[15] Ji, C., Jia, X., Huang, X., Zhou, S., Chen, G., & Zhu, Y. (2024). FusionNet: Detection of Foreign Objects in Transmission Lines During Inclement Weather. IEEE Transactions on Instrumentation and Measurement.

[16] Luo, Y., Yu, X., Yang, D., & Zhou, B. (2023). A survey of intelligent transmission line inspection based on unmanned aerial vehicle. Artificial Intelligence Review, 56(1), 173-201.

[17] Weng, B., Gao, W., Zheng, W., & Yang, G. (2021). Newly designed identifying method for ice thickness on high‐voltage transmission lines via machine vision. High Voltage, 6(5), 904-922.

[18] Ma, F., Liu, H., Wang, J., Jia, R., Wang, B., & Ma, H. (2024). A Refined Identification Method for the Hidden Dangers of External Damage in Transmission Lines Based on the Generation of a Vanishing Point-Driven Effective Region. Processes, 12(9), 1904.

[19] Ebrahimi, H., Golshannavaz, S., Yazdaninejadi, A., & Pouresmaeil, E. (2025). A Hidden Surveillant Transmission Line Protection Layer for Cyber-Attack Resilience of Power Systems. IEEE Open Journal of the Industrial Electronics Society.

[20] Yin, X., Zuo, Y., & Fu, G. (2024). Design of intelligent detection method for electricity transmission line equipment defect based on data mining algorithm. International Journal of Thermofluids, 24, 100814.

[21] Liu, H., Chen, Y., Cui, N., Xu, D., & Li, J. (2021). An effective data fusion model for detecting the risk of transmission line in smart grid. IEEE Internet of Things Journal, 9(22), 22256-22266.

[22] Wang, L., Li, H., Lu, X., Li, X., Zhang, J., Wang, X., & Chen, C. (2022). Design of intelligent monitoring system in galloping power transmission line. Sensors, 22(11), 4197.

[23] Gopakumar, P., Mallikajuna, B., Reddy, M. J. B., & Mohanta, D. K. (2018). Remote monitoring system for real time detection and classification of transmission line faults in a power grid using PMU measurements. Protection and Control of Modern Power Systems, 3(2), 1-10.

[24] Zheng, W., Li, C., Yang, B., & Sun, X. (2019, November). Identification of hidden dangers in transmission line corridors based on hybrid algorithms. In Journal of Physics: Conference Series (Vol. 1346, No. 1, p. 012042). IOP Publishing.

[25] Zheng, W., Shang, J., Chang, A., Song, Y., & Xiao, Y. (2023, April). Research on hidden danger identification of external damage of high voltage overhead transmission lines. In Eighth International Conference on Energy Materials and Electrical Engineering (ICEMEE 2022) (Vol. 12598, pp. 746-752). SPIE.

[26] Liu, L., Du, R., & Liu, W. (2019). Flood distance algorithms and fault hidden danger recognition for transmission line towers based on SAR images. Remote Sensing, 11(14), 1642.

[27] Yang, Y., Li, Z., Liu, N., Su, Y., Yan, X., & Tao, H. (2023, October). Research and Design of Hidden Trouble Target Reconfirmation and Repeated Hidden Trouble Target Filtering Technology in Transmission Line Online Monitoring. In International Conference on Heterogeneous Networking for Quality, Reliability, Security and Robustness (pp. 3-14). Cham: Springer Nature Switzerland.

[28] Lodhi, E., Wang, F. Y., Xiong, G., Dilawar, A., Tamir, T. S., & Ali, H. (2022). An AdaBoost ensemble model for fault detection and classification in photovoltaic arrays. IEEE Journal of Radio Frequency Identification, 6, 794-800.

[29] Sun Qizhen, Ai Fan,Liu Deming, Cheng Jianwei, Luo Hongbo, Peng Kuan... & Shum Perry Ping. (2017). M-OTDR sensing system based on 3D encoded microstructures. Scientific reports,7(1-4),41137.

[30] Robert Cep, Muniyandy Elangovan, Janjhyam Venkata Naga Ramesh, Mandeep Kaur Chohan & Amit Verma. (2025). Convolutional Fine-Tuned Threshold Adaboost approach for effectual content-based image retrieval. Scientific reports,15(1),9087.